Neotectonics, geodesy, and seismic hazard in the Northern Walker Lane of Western North America: Thirty kilometers of crustal shear and no strike-slip?

Steven G. Wesnousky [a,*], Jayne M. Bormann [b], Corné Kreemer [b], William C. Hammond [b], James N. Brune [c]

[a] Center for Neotectonic Studies, MS 169, University of Nevada, Reno 89557, United States
[b] Nevada Geodetic Laboratory, Nevada Bureau of Mines and Geology, 89557, United States
[c] Nevada Seismological Laboratory, University of Nevada, Reno 89557, United States

ABSTRACT

Roughly 30 km of cumulative right-lateral crustal displacement and 5–6 mm/yr of the ongoing relative right-lateral motion between the Pacific and North American plates are observed in the northern Walker Lane. The right-lateral shear has been accommodated in large part by the development of a set of discontinuous, en echelon, normal fault-bounded basins and perhaps significant vertical axis rotations of the intervening crust. The observations provide an illustrative example of how large amounts of crustal shear may be accommodated in the absence of strike-slip faults and point to difficulties attendant to melding geologic and geodetic observations in the analysis of seismic hazard. In this particular case, the assumption that all geodetically observed shear across the area will be recorded by earthquake displacements may be flawed.

© 2012 Elsevier B.V. All rights reserved.

1. Introduction

The Walker Lane is a northwest trending zone of discontinuous active faults and disrupted topography that sits between the Sierra Nevada on the west and the north–northeast trending faults and ranges of the Great Basin to the east (Fig. 1). About one fifth of the ongoing ~50 mm/yr of right-lateral transform motion across the Pacific-North American plate boundary is accommodated east of the Sierra Nevada, mostly localized within the Walker Lane (e.g., Fig. 2, Bennett et al., 1999; Bennett et al., 2003; Hammond and Thatcher, 2004; Oldow et al., 2001; Thatcher et al., 1999). The occurrence of both normal and strike-slip faulting within the Walker Lane indicate transtensional deformation (Stewart, 1988; Taylor and Dewey, 2009; Unruh et al., 2003). We combine neotectonic and geodetic observations in the region that includes the Lake Tahoe, Carson, Smith, Mason, Antelope, Bridgeport and Walker Lake basins to examine the pattern and rate of strain accumulation across the northern Walker Lane. The sum of observations leads to an illustrative example of how tens of kilometers of localized shear may be accommodated in the absence of strike-slip faults and of the difficulty in melding geologic and geodetic observations in the analysis of seismic hazard.

We begin by placing the area of study in a regional context, follow with a description of the neotectonic and geodetic characteristics of the basins, then use the observations to discuss the manner in which crustal strain in the region is accommodated and the implications for seismic hazard analysis.

2. Regional context

The major active faults and physiography of the Walker Lane are shown in Fig. 1. Faults of the southern Walker Lane include the Sierra Nevada range front normal fault and the north–northwest trending right-lateral Owens Valley, White Mountains, Panamint–Hunter Mountain–Saline Valley, and Fish Lake Valley–Furnace Creek–Death Valley, and Stateline fault systems. Cumulative right-lateral slip across the faults is greater than ~50 km (e.g., Guest et al., 2007; McQuarrie and Wernicke, 2005; Niemi et al., 2001; Snow and Wernicke, 1989, 2000; Wernicke et al., 1988). Easterly striking left-lateral faults at the northern extent of the southern Walker Lane comprise a right-step across which slip is transferred northward to the major northwest-trending right-lateral strike-slip faults of the central Walker Lane, which include the Agai-Pai, Indian Head, Gumdrop, Benton Springs, and Petrified fault systems. The faults record at least 34 km of cumulative right offset (Ekren and Byers, 1984; Hardyman, 1984). A further 5–10 km of right-lateral slip may by recorded on the fault that bounds the west side of Walker Lake basin (Ekren et
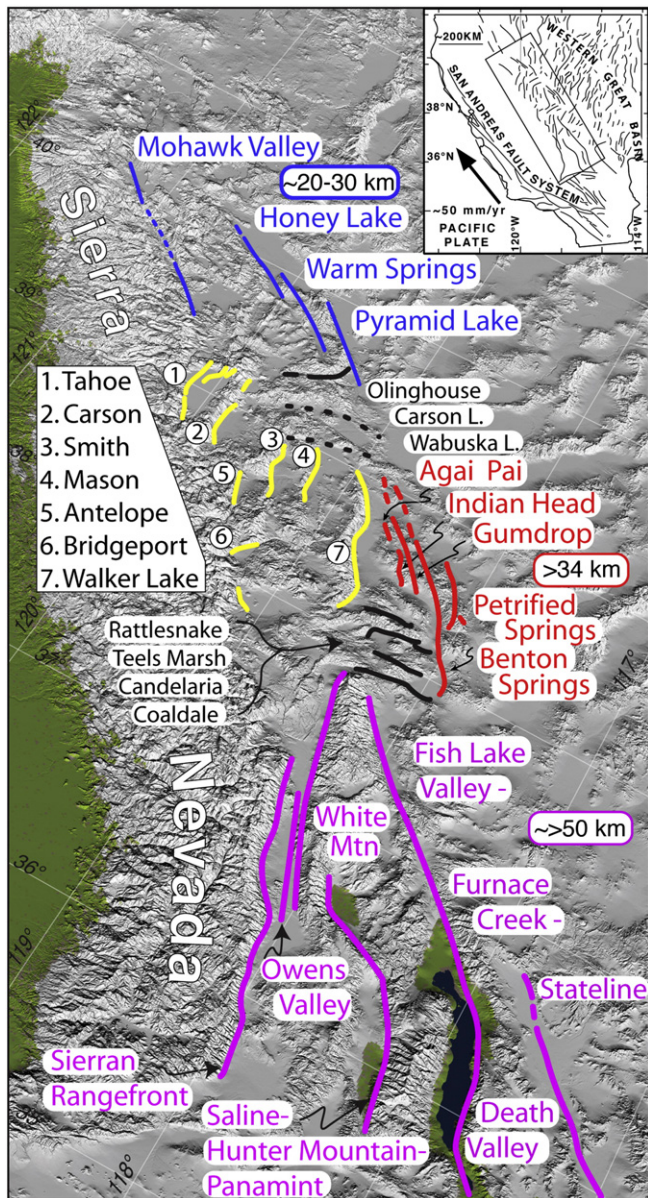
Fig. 1. Annotated digital elevation model viewed obliquely and northward along Walker Lane. Values of cumulative right-slip (km) across each the southern (magenta), central (red), and northern (blue) Walker Lane fault systems are annotated and adapted from summary of Wesnousky (2005b). East–west striking left-lateral faults (solid) and structural lineaments (dashed) are black. Major structural basins and bounding normal faults (yellow) between the central and northernmost Walker Lane are numbered and labeled. Inset shows location in context of San Andreas and Western Great Basin fault systems. (For interpretation of the references to color in this figure legend, the reader is referred to the web version of this article.)

al., 1980). The en echelon Pyramid Lake, Warm Springs Valley, and Honey Lake fault systems define the northernmost Walker Lane and record ~20–30 km of total right slip (Faulds et al., 2005; Henry and Faulds, 2010). Cumulative slip on the Mohawk Valley fault to the west is not well documented and suggested to be on the order of 1 kilometer (Faulds et al., 2005; Saucedo and Wagner, 1992). We focus on the region that separates and sits largely to the west of the right-lateral fault systems of the central and northernmost Walker Lane. The area is defined by a set of seven normal fault-bounded basins arranged in a generally en echelon and left-stepping manner (Fig. 1: the Tahoe, Carson, Smith, Mason, Antelope, Bridgeport and Walker Lake basins), and the east trending left-lateral Olinghouse fault (e.g. Briggs and Wesnousky, 2001) and Carson and Wabuska lineaments.

The Carson and Wabuska lineaments are expressed by near-alignment of valleys and mountain ranges and have been considered zones of left slip (Cashman and Fontaine, 2000; Rogers, 1975). The normal fault-bounded basins are the most profound and active structural elements in the region between and to the west of the major strike-slip faults of the central and northern Walker Lane. One may infer from the estimates of cumulative offset to the north and south of this region that a minimum of ~20 to 30 km of right-lateral strike-slip has been accommodated across this section of the Walker Lane in the absence of well-developed strike-slip faults. A similar type of discrepancy is reported in the southern Walker Lane at Yucca Mountain where Quaternary strain absorbed by faulting is insufficient to explain ongoing geodetic motions (Wernicke et al., 2004; Hill and Blewitt, 2006).

3. The basins: neotectonic and geodetic characteristics

3.1. Fault slip rates

The *Lake Tahoe Basin* is the westernmost of the fault-bounded basins in the northern Walker Lane (Fig. 3). The basin is bounded and cut by northerly striking and east-dipping active normal faults. Employing subaqueous geophysics and coring methods, the investigations of Brothers et al. (2009), Dingler et al. (2009), and Kent et al. (2005) show cumulative vertical offset across faults bounding and cutting the basin during the last 20 kyr to 60 kyr is about 0.85–1.7 mm/yr. *Carson Valley* is bounded on the western side by the east-dipping Genoa normal fault. Ramelli et al. (1999) conducted paleoseismic investigations at 3 sites along the fault, each revealing normal displacement on a steeply dipping fault. They identified two 3–5.5 m surface-rupturing earthquake displacements at about 500–600 cal BP and 2000–2200 cal BP, respectively, and on that basis interpret a late Holocene dip-slip rate of 2–3 mm/yr for the central segment of the Genoa fault. More recently Rood et al. (2011a) interpret a 0.3–0.7 mm/yr dip slip rate for the southern section of the Genoa fault averaged over the late Pleistocene based on cosmogenic dating of older vertically offset glacial surfaces near the southern limit of the Carson basin. In *Smith Valley*, fault scarps cut young alluvium along the length of the east-dipping range-bounding fault. A trench across the scarp shows that the last surface rupture produced ~3.5 m of normal displacement and occurred about 3530 ± 82 cal BP. A 10 to 20 m vertical offset of a 60 to 80 ka fan surface places the late Pleistocene vertical slip rate of the fault at between about 0.1 mm/yr and 0.3 mm/yr (Wesnousky and Caffee, 2011). A paleoseismic investigation on the west side of *Antelope Valley* reports two Holocene surface ruptures showing 3.1 and 3.5 m normal displacement and an estimated 0.7 mm/yr Holocene dip-slip rate for the east-dipping normal fault. We are aware of no published reports on the slip rate of the normal fault bounding the west side of *Mason Valley*. Our observations show vertical separation of the largest alluvial scarp along the fault trace to be less than 10 m in height and the offset surface to be mantled by a soil displaying a Bt horizon and Stage 3 carbonate. Such soil characteristics indicate that the surface is older than Holocene and is mid- to late Pleistocene in age (~30–175 kyr) (Bell, 1995; Koehler and Wesnousky, 2011). The observations suggest a maximum bound on the vertical slip rate of 0.3 mm/yr. Using cosmogenic dating techniques and scarp profile measurements on offset glacial deposits, Rood et al. (2011a) estimate the dip-slip rate of the fault bounding the northwest flank of *Bridgeport Valley* at 0.2–0.4 mm/yr over the last ~20 ky and ~150 ky. Surface morphology and a trench excavated across the Wassuk range-bounding fault at a site on the west side of *Walker Lake* basin record an ~5.5–7 m scarp resulting from at least two normal displacement earthquakes on a steeply dipping fault during the last ~9400 years (Bormann et al., in press; Demsey, 1987), suggesting a Holocene vertical slip rate on the order of 0.6–0.8 mm/yr. An older abandoned fan surface along

the same fault is displaced vertically ~40 m and cosmogenic nuclide analysis of large boulders on the surface place the age of the surface at 112.9 ± 12.5 ka (Bormann et al., in press). Dividing the offset by the age yields a late Pleistocene vertical slip rate for the fault of ~0.3–0.4 mm/yr over the longer period.

Earthquake displacements reported in the trenches along the Wassuk, Smith Valley, Carson (Genoa), and Antelope basin-bounding faults are dip-slip. The steep range fronts, triangular facets, discontinuous and sinuous traces, and consistent presence of scarps showing down-to-the-basin displacement further attest to dip-slip motion on the range-bounding faults. The same is true for the Tahoe, Bridgeport and Mason basins. Geologic observations thus indicate that the horizontal projection of slip along each of the basin bounding faults is dominantly normal to the average strike of the respective faults.

3.2. Horizontal components of fault slip rate

To compare the reported rates of displacement for the basin bounding faults to the geodetically measured deformation, the preceding vertical and dip-slip rates are converted to horizontal extension rates as explained and given in Table 1 for each fault. The azimuth and horizontal rate of extension are annotated and delineated by the two-headed black arrows adjacent to each of the major range-bounding faults in Fig. 3. The points of the two arrowheads span the minimum and maximum bounding estimates of horizontal extension for the respective faults. The extension directions are taken to be perpendicular to the average strike of the respective faults. The arrows are placed adjacent to the location of the respective slip rate studies, except for Tahoe where the value is an average across several submarine faults.

3.3. Geodesy

Our recording and analysis of GPS stations from the EarthScope Plate Boundary Observatory network and the MAGNET network operated by the University of Nevada, Reno define the crustal deformation

Table 1
Horizontal extension rates on major range-bounding faults derived from geology.

#	Basin	Vertical slip rate	Dip-slip rate	Horizontal extension rate[a]
1	Tahoe[b,c,d]	0.85–1.7		0.5–1.7
2	Carson[e]		2–3	0.7–1.7 (55°–70°)
2	Carson[f]		0.3–0.7	0.1–0.5 (50°–70°)
3	Smith[g]	0.125–0.33		0.1–0.3
4	Mason[h]	0.3		0.2–0.3
5	Antelope[i]		~ 0.7	0.35 (60°)
6	Bridgeport[f]		0.2–0.4	0.1–0.3 (50°–70°)
7	Walker (central)[j,k]	~0.8		0.5–0.8
7	Walker (north)[j,l]	~0.4		0.2–0.4

[a] Where only vertical slip rates are reported, the horizontal extension rate is equal to the vertical separation rate divided by the tangent of the fault dip. Based on the abrupt and steep nature of the associated range fronts (Fig. 3) and the observations of fault dip commonly observed in paleoseismic trench studies, the calculation of horizontal extension rate in these cases assumes fault dips are between 45° and 60°. Where fault dip-slip rates are reported, the horizontal extension rate is equal to the reported dip-slip rates times the cosine of the fault dips reported by the respective authors (in parentheses).

[b] Kent et al. (2005).
[c] Brothers et al. (2009).
[d] Dingler et al. (2009).
[e] Ramelli et al. (1999).
[f] Rood et al. (2011a).
[g] Wesnousky and Caffee (2011).
[h] Authors observation (unpublished).
[i] Sarmiento et. al. (2011).
[j] Bormann et al. (in press).
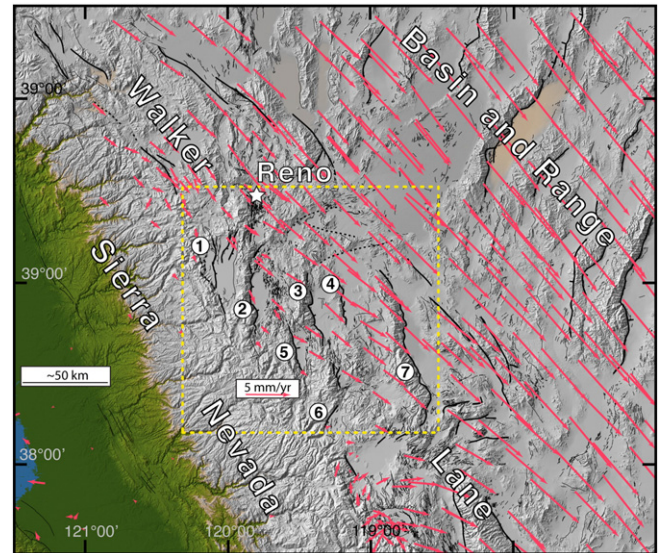[k] Demsey (1987).
[l] Surpless (2010).

Fig. 2. Velocity field derived from Global Positioning System (GPS) across northern Sierra Nevada and Walker Lane, and extending into the western Basin and Range. Vectors are plotted with respect to Sierra Nevada. Velocities derived from GPS stations of EarthScope's Plate Boundary Observatory network and the MAGNET network operated by the University of Nevada, Reno (star) define displacement using methodology outlined in Hammond et al. (2011). Major mapped active faults are black lines. Basins numbered as in Fig. 1. Yellow dashed box outlines area of Fig. 3.

field in this region to a greater resolution than was previously possible. The red vectors in Figs. 2 and 3 represent the estimated velocity of each GPS station with respect to the Sierra Nevada and are calculated using the methodology outlined in Hammond et al. (2011). The vast majority of measurements are made between 2004 and 2010. A fewer number of stations (12%) have been in operation longer, up to a period of 15 years. Implicit to the ensuing analysis is that these velocities represent long-term trends.

We focus our attention on the area of Fig. 3. The vectors are consistently oriented to the southeast and increase in magnitude as one progresses northeastward from the Sierra Nevada. The pattern defines to first order a simple right-lateral shear field oriented along the trend of the Walker Lane. The rate of right-lateral strain accumulation between station LANT in the Sierra Nevada and station RAIN about 120 km to the northeast is 5–6 mm/yr (Figs. 3 and 4A). The GPS velocities also tend to increase in magnitude from northwest to southeast indicating that there exists an additional component of stretching or extension along the axis of this portion of the Walker Lane equal to ~2 mm/yr between station BOCA to the northwest and LUCK in the southeast (Figs. 3 and 4b). The along-strike extension in the Walker Lane was earlier recognized by Bennett et al. (2003) and can be attributed to the GPS vectors and shear field being oriented slightly oblique to the northeastern boundary of the Sierra Nevada.

From the discrete velocity measurements in Fig. 4, we derive a continuous velocity gradient tensor field across the area using the velocity and strain rate interpolation method of Beavan and Haines (2001). The velocity gradient tensor field is then used to create a discrete interpolated velocity field at 0.01° intervals. Assuming that strain accumulating within the 20–30 km volume centered about the respective faults is ultimately relaxed by fault slip, we approximate the fault normal and parallel components of slip rate by differencing the interpolated velocity field in a 20–30 km transect perpendicular to each fault. The calculations and method are detailed in the Supplemental information. The calculated rates of fault normal (horizontal extension) and strike-slip are annotated and shown in Fig. 3 with violet and blue arrows, respectively, and are summarized in Table 2.
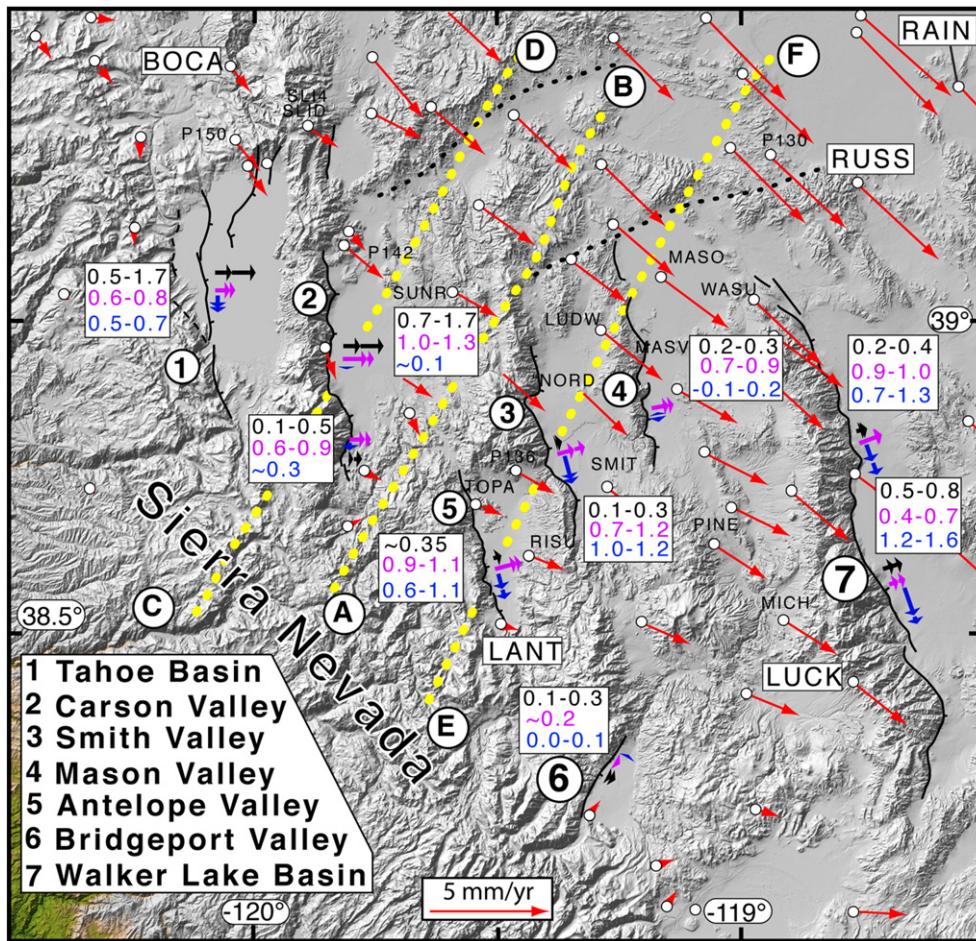
Fig. 3. Physiographic and fault map of area of interest in northern Walker Lane shows major structural basins (numbered), active basin-bounding faults (thick black lines), and geodetic displacement field (red arrows). Shown in white boxes are geologically determined values of fault-normal extension (black-upper text), geodetic estimates of fault-normal extension (magenta-middle text) and geodetic estimates of fault-parallel strike-slip (blue-lower text) rates along each of the basin bounding faults. Two-headed arrows schematically show ranges of same values and correspond in arrangement and color to the values in boxes. The geologically determined extension rate arrows are placed adjacent to the sites of studies except for Lake Tahoe where the estimate is an average value across several submarine faults. Dotted (yellow) lines define paths AB, CD, and EF discussed in text. GPS stations LANT, RAIN, BOCA and LUCK are the endpoints of profiles shown in Fig. 4. Area of this figure is outlined by yellow dashed box in Fig. 2. (For interpretation of the references to color in this figure legend, the reader is referred to the web version of this article.)

While block models are often used to account for strain and rotations in geodetic studies (e.g. Hammond et al., 2011; McCaffrey, 2002), we have instead used the strain field local to the fault to estimate the geodetic slip rate. This method does not assume the specifics of fault connections to form contiguous blocks, nor does it enforce regional kinematic consistency, so the results provide geodetic slip rates that are independent of the effects of predefined blocks.

4. Discussion

4.1. Rates of fault slip: geology versus geodesy

The major active faults in our region of study are those bounding the large structural basins. The bounds on geologically determined horizontal extension rates along each of the range-bounding faults generally overlap the values of extension predicted from geodesy (Fig. 3). Differences do exist for the faults bounding Antelope, Smith and Mason valleys, where geodetic extension rates are twice those estimated from geology, though the differences separating the ranges of geologically and geodetically derived values in an absolute sense are only about 0.5 mm/yr or less. To this order then, geodesy and geology are providing generally similar measures of the normal component of fault slip rate on these range-bounding faults.

Unlike geologic observations, geodetic measurement predicts right-lateral strike-slip along some of the basin-bounding faults that is equal to or greater than the extensional component of slip. The predicted strike-slip motion appears to conflict with geologic observations indicating motion along the range-bounding faults is primarily dip-slip. The related questions then arise to 1) how and where the strike-slip component of deformation registered by geodesy is recorded in the geologic record and 2) to what degree may one account for the total geodetic velocity field by displacement on the basin-bounding faults? The paths AB, CD, and EF in Fig. 3 are drawn to illustrate and address the questions.

Each of the paths AB, CD, and EF are drawn transverse to the principal direction of simple shear and represent paths of line integrals over which cumulative fault slip across the area may be summed (e.g., Humphreys and Weldon, 1994). No faults are intersected by path AB and accordingly no part of the geodetic velocity field may be accounted for with displacement on major range-bounding faults. In contrast paths CD and EF cross major range-bounding faults. Path CD crosses only the Carson Valley that is bounded on its western flank by the Genoa fault. The maximum horizontal extension produced by normal displacement on the fault is ~1.7 mm/yr. The slip azimuth is oblique to the direction of simple shear defined by GPS observation and thus is not oriented optimally to accommodate the shear. At most, fault displacement recognized from geologic
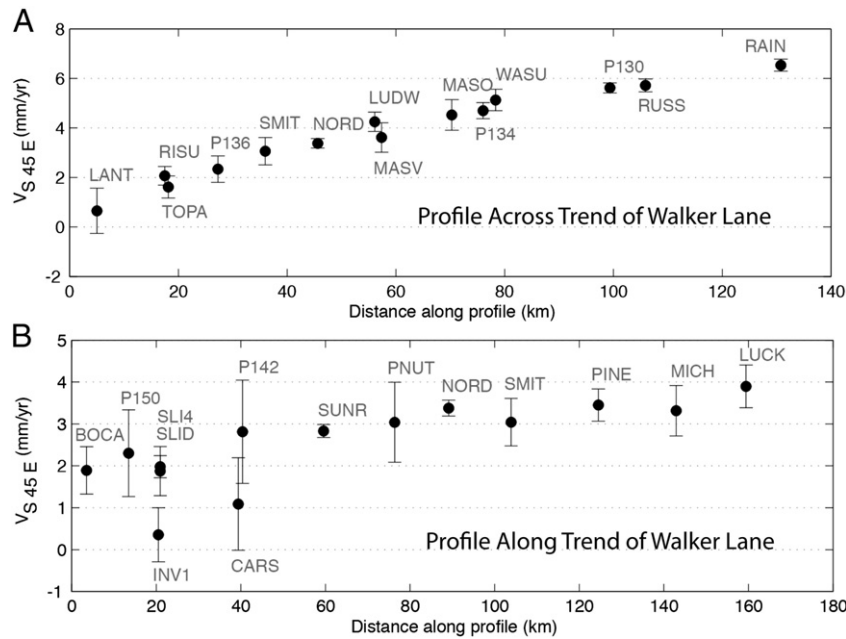
Fig. 4. GPS displacement rates projected (A) across and (B) along the trend of the Walker Lane. Station locations are shown in Fig. 3.

observations can account for less than ~2 mm/yr of the ~5 mm/yr that is registered geodetically across the transect. The maximum number of faults that may be crossed is defined by path EF. The three faults that are crossed by the transect each record geologically-determined fault normal extension rates less than ~0.5 mm/yr, and again the slip azimuths are not oriented optimally to account for the geodetic shear field. Geologic slip rates account for no more than ~1.5 mm/yr of the 5 mm/yr geodetic shear budget between stations LANT and RAIN. It may alternately be suggested that geologic rates of extension on the three faults underestimate the actual extensional displacement rates because the geodetic estimates of fault normal extension are larger, each showing maximum bounds of ~1 mm/yr. Assuming the suggestion is correct, and we instead use the geodetically derived values of fault-normal extension, slip on the range-bounding faults would still account for less than 50% of the geodetic shear field because the extension vectors are quite oblique to the sense of geodetic shear. If one further computes the vector sum of geodetically-determined fault normal and parallel components of slip for each of the three faults, the cumulative slip rate reaches ~4 mm/yr, approaching the ~5 mm/yr of geodetic shear being recorded between stations LANT and RUSS. The sum of observations indicates, regardless of whether geologic or geodetic observations are favored, that the accommodation of the shear field in this region cannot be accommodated solely by normal displacement on the range-bounding faults and that the amount of the geodetically observed deformation field that may be accounted for on basin-bounding faults is dependent on the path one follows across the region.

4.2. Modes of strain accommodation

We highlight three key observations: 1) there are no major northwest-trending strike-slip faults traversing the study area, 2) geologic and geodetic slip rates on the observed major range-bounding faults are insufficient to explain the entirety of the geodetically observed shear across the region, and 3) geodetic measurements reveal a significant component of NW–SE extension parallel to the Walker Lane (Fig. 4 and Bennett et al., 2003). We infer from the observations that the displacement field across the region is taken up by a combination of vertical axis rotations, southeastward translation of crustal blocks approximately parallel to the Walker Lane, and opening of the en echelon set of basins. The idea is visualized in the model shown on the left of Fig. 5. A block of wax is heated and the central portion of the block is subject to a right-lateral shear with a small component of extension. Subsequently, an identical block of wax is heated and ice applied to the surface to create a 'brittle crust' and subjected to the same shear. The result is a broad zone of en echelon crustal blocks and basins. The blocks have generally undergone clockwise vertical axis rotations and the basins record a component of extension and block translation along the axis of principal shear.

Table 2
Rates of fault-parallel slip and fault-perpendicular horizontal extension derived from geodesy.

#	Basin	Fault trend (°)	Velocity east	Velocity south	Fault perpendicular extension (mm/yr)	Fault-parallel shear (mm/yr)
1	Tahoe	0	0.6–0.8	0.5–0.7	0.6–0.8	0.5–0.7
2	Carson Central	0	1.0–1.3	0.0–0.1	1.0–1.3	~0.1
2	Carson South	0	0.6–0.9	~0.3	0.6–0.9	~0.3
3	Smith	−15	0.9–1.5	0.8–0.9	0.7–1.2	1.0–1.2
4	Mason	−10	0.7–0.9	0.1–0.2[a]	0.7–0.9	0.1[b]–0.2
5	Antelope	−15	1.1–1.4	0.7–1.1	0.9–1.1	0.6–1.1
6	Bridgeport	30	0.2–0.3	0.0–0.1	~0.2	0.0–0.1[a]
7	Walker Central	−15	0.7–1.1	1.0–1.4	0.4–0.7	1.2–1.6
7	Walker North	−15	1.1–1.3	0.5–1.0	0.–1.0	0.7–1.3

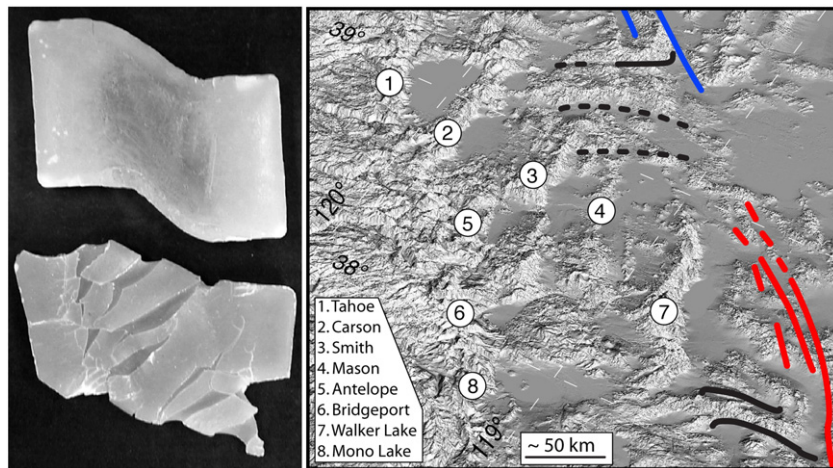[a] North.
[b] Left-lateral.

Fig. 5. (Left) Model to visualize accommodation of strain and development of basins in northern Walker lane. The upper is a block of wax has been heated to become ductile and subjected to transtensional right-lateral shear. Ice has been applied to the surface of lower wax block to create brittle upon ductile layer, and then subjected to same shear. The transtensional shear results in a zone of deformation displaying rotation of 'crustal blocks', an en echelon arrangement of asymmetric 'basins', observable extension along the axis of shear, and the ability to locally traverse the entire zone of shear without encountering a major fault structure. (Right) Oblique view of study area illustrates the en echelon arrangement and triangular shape of basins nested along the east edge of the Sierra Nevada. Black and colored lines are portions of Walker Lane faults shown in Fig. 1.

The model is not presented as a perfect analog to crustal deformation processes in the earth but it does serve to illustrate how transtension can lead to development of the en echelon arrangement and physiographic expression of the basins we observe in the northern Walker Lane (Fig. 5), as well as the geodetically observed extension oriented along the trend of the Walker Lane (Fig. 4B). The en echelon arrangement and distinct triangular form of the Bridgeport, Antelope, and Tahoe basins situated along the eastern boundary of the Sierra Nevada (Fig. 5) is markedly similar to that observed in the wax model. The triangular basin shapes imply along strike variation of slip rate on the basin-bounding faults and, in turn, possible vertical axis rotations of the adjacent crustal blocks.

The idea that crustal rotation provides a mechanism to accommodate displacement in a zone of shear is not new (e.g., Garfunkel and Ron, 1985; Nicholson et al., 1986). Within the Walker Lane, Cashman and Fontaine (2000) have documented paleomagnetic clockwise vertical axis rotations in the terrane just to the east of the basins and between the Carson and Olinghouse lineaments. Vertical axis rotations have also been interpreted in the region of left-lateral cross-faults between the southern and northern Walker Lane (Fig. 1) on the basis of paleomagnetic measurements (e.g. Petronis et al., 2009; Rood et al., 2011b) and the spatial relationship of basins to the left-lateral faults (Wesnousky, 2005a). The possibility of terrane rotations within the region of fault-bounded basins could equally be tested with paleomagnetics. We are aware of no similar studies in the area of fault bounded basins studied here.

4.3. Seismic hazard

A general premise of modern seismic hazard analysis is that accumulation of crustal strain measured geodetically should ultimately be released as brittle failure of the crust and, analogously, geologic rates of displacement on active faults should be in accord with geodetic measures of strain accumulation across an area. In this regard, the characteristics of deformation we have described in the northern Walker Lane result in a conundrum. The accommodation of geodetically observed shear in this region may not be accounted for solely by displacement on major active faults. Additionally, the mismatch may not be attributed solely to errors in geologists' measures of slip rate or the possibility that major active fault structures remain unidentified; one may traverse this portion of the Walker Lane without encountering a major fault structure.

The major fault systems within the area exhibit morphology consistent with primarily normal displacement. The azimuths of fault normal displacements are misaligned to geodetic velocity field and estimated rates of fault-slip are insufficient to account for the magnitude of geodetically observed shear across the area. Yet the geologically estimated fault-normal extension rates are in general accord with those predicted from interpolation of the geodetic velocity field, albeit geodetic observation implies most faults should also show a component of fault parallel slip that is not recognized by geologists.

Accepting the initial premise of this section leads to the inference that geologists have yet to recognize evidence of strike-slip along the major basin-bounding faults or that a large portion of the shear deformation is accommodated by crustal rotations in the absence of shear strain accumulation. Both seem likely. For example, the approximate agreement of fault normal extension observed geologically to that predicted geodetically is an argument that geodesy is providing an accurate measure of strain accumulation in the volume around faults. If so, it follows that the predicted values of fault-parallel shear are accurate as well and that it is simply not recognized or quantified along the main basin-bounding faults. Suggestions of right-lateral slip have for example been reported along the range-front faults bounding Walker Lake and Antelope Valley (Sarmiento, 2010; Wesnousky, 2005a), though robust evidence of oblique slip has yet to be documented. Strike-slip displacement may also be hidden in the basin sediments if the strike-slip and dip-slip components are partitioned such that dip slip is recorded on the main basin bounding faults and the strike-slip displacement is partitioned outboard in the depositional basins (e.g., King et al., 2005; Wesnousky and Jones, 1994), perhaps unrecognized or poorly recorded because of the lack of vertical offset and slow slip rates. Allowing that rates of strike-slip along basin-bounding faults approach the magnitude of reported normal displacements, the conundrum nonetheless remains: fault slip rates on the major basin-bounding faults cannot account for the entirety of the geodetic displacement field. The inability to account for the strain accumulation budget by fault slip and the discontinuous and en echelon arrangement of basin-bounding faults thus seems to require that crustal block rotations play a significant role in accommodating right-lateral deformation across the region.

The consequence of block rotations to estimations of seismic hazard analysis may be large. Block rotations will contribute to the right-lateral displacement across the northern Walker Lane in the absence of internal strain accumulation. The assumption that the entire

~5 mm/yr geodetic shear registered across the region is ultimately recorded in earthquake displacements is likely incorrect and will lead to an overestimation of seismic hazard in the region. The geology shows that basin-bounding faults have been the major source of repeated surface-rupturing earthquakes in the region. Thus, while there remains a mismatch of geologic rates of fault displacement to that apparent from geodesy, the actual level of seismic hazard is probably better reflected in the assumption that the potential size and recurrence time of earthquakes is a respective function of the lengths and rates of slip on the major faults of the region. It is not clear how the suspected rotation is ultimately accommodated further to the east of the study area. These assumptions also ignore the possibility that some component of Walker Lane shear is accommodated aseismically.

5. Summary and conclusion

The northern Walker Lane provides an insightful illustration of the complexity that may accompany the accommodation of simple shear. Here, the ~30 km of right-lateral cumulative strike slip has been accommodated in the absence of any well-developed strike-slip faults. Rather, the deformation has been taken up primarily by the development of a set of en echelon normal fault bounded basins and an apparently significant amount of crustal rotation. If the pattern of cumulative strain accommodation remains active today, a component of geodetic deformation recorded across the region is likewise also reflecting block rotations. If so, the assumption that all geodetically observed shear across the region will be accommodated by earthquakes will likely lead to overestimates of the level of seismic hazard in the area.

Acknowledgments

Appendix A. Supplementary data

Supplementary data to this article can be found online at doi:10.1016/j.epsl.2012.02.018.

References

Beavan, J., Haines, J., 2001. Contemporary horizontal velocity and strain rate fields of the Pacific-Australian plate boundary zone through New Zealand. J. Geophys. Res. 106, 741–770.

Bell, J.W., 1995. Quaternary geologic map of the Mina quadrangle, Nevada. Nevada Bureau of Mines and Geology Field Studies Map 10, 1:24,000.

Bennett, R.A., Davis, J.L., Wernicke, B.P., 1999. Present-day pattern of Cordilleran deformation in the western United States. Geology 27, 371–374.

Bennett, R.A., Wernicke, B.P., Niemi, N.A., Friederich, A.M., Davis, J.L., 2003. Contemporary strain rates in the northern Basin and Range province from GPS data. Tectonics 22 (2). doi:10.1029/2001TC001355.

Bormann, J.M., Surpless, B.E., Caffee, M.W., Wesnousky, S.G., 2012. Holocene earthquakes and late Pleistocene slip rate estimates on the Wassuk Range fault zone, Nevada, USA. Bull. Seismol. Soc. Am. 102–104.

Briggs, R.W., Wesnousky, S.G., 2001. Paleoseismic evidence for repeated Holocene earthquakes on the Olilnghouse fault zone, western Nevada. EOS Trans. (supplement) 82, F935.

Brothers, D.S., Kent, G.M., Driscoll, N.W., Smith, S.B., Karlin, R., Dingler, J.A., Harding, A.J., Seitz, G.G., Babcock, J.M., 2009. New constraints on deformation, slip rate, and timing of the most recent earthquake on the West Tahoe-Dollar Point Fault, Lake Tahoe Basin, California. Bull. Seismol. Soc. Am. 99, 499–519.

Cashman, P.H., Fontaine, S.A., 2000. Strain partitioning in the northern Walker Lane, western Nevada and northeastern California. Tectonophysics 326, 111–130.

Demsey, K., 1987. Holocene faulting and tectonic geomorphology along the Wassuk Range, west central Nevada. M.S. Thesis, University of Arizona, Tucson, 62 pp.

Dingler, J., Kent, G., Driscoll, N., Babcock, J., Harding, A., Seitz, G., Karlin, B., Goldman, C., 2009. A high-resolution seismic CHIRP investigation of active normal faulting across Lake Tahoe Basin, California-Nevada. Geol. Soc. Am. Bull. 121, 1089–1107.

Ekren, E.B., Byers, F.M., 1984. The Gabbs Valley Range — a well-exposed segment of the Walker Lane in west-central Nevada. In: Lintz Jr., J. (Ed.), Geological Society of America, Guidebook, Annual Meeting, Reno, Nevada, pp. 203–215.

Ekren, E.B., Byers, F.M., Hardyman, R.F., Marvin, R.F., Silberman, M.L., 1980. Stratigraphy, preliminary petrology, and some structural features of Tertiary volcanic rocks in the Gabbs Valley and Gillis Ranges. U.S. U.S. Geol. Surv. Bull. 1464, 1–54.

Faulds, J.E., Henry, C.D., Hinz, N.H., 2005. Kinematics of the northern Walker Lane: an incipient transform fault along the Pacific-North American plate boundary. Geology 33, 505–508.

Garfunkel, Z., Ron, H., 1985. Block rotation and deformation by strike-slip faults. 2. The properties of a type of macroscopic discontinuous deformation. J. Geophys. Res. 90, 8589–8602.

Guest, B., Niemi, N., Wernicke, B., 2007. Stateline fault system: a new component of the Miocene-Quaternary Eastern California shear zone. Geol. Soc. Am. Bull. 119, 1337–1346.

Hammond, W.C., Thatcher, W., 2004. Contemporary tectonic deformation of the Basin and Range province, western United States: 10 years of observation with the Global Positioning System. J. Geophys. Res. Solid Earth 109.

Hammond, W.C., Blewitt, G., Kreemer, C., 2011. Block modeling of crustal deformation of the northern Walker Lane and Basin and Range from GPS velocities. J. Geophys. Res. Solid Earth 116.

Hardyman, R.F., 1984. Strike-slip, normal, and detachment faults in the northern Gillis Range, Walker Lane of west-central Nevada. In: Lintz Jr., J. (Ed.), Geological Society of America, Guidebook, Annual Meeting, Reno, Nevada, pp. 184–199.

Henry, C.D., Faulds, J.E., 2010. Ash-flow tuffs in the Nine Hill, Nevada, paleovalley and implications for tectonism and volcanism of the western Great Basin, USA. Geosphere 6, 339–369.

Humphreys, E.D., Weldon, R.J., 1994. Deformation across the western United States: a local estimate of Pacific-North American transform deformation. J. Geophys. Res. 99, 19975–20010.

Hill, E.M., Blewitt, G., 2006. Testing for fault activity at Yucca Mountain, Nevada, using cross-validated GPS results from the Bargen network. Geophys. Res. Lett. 33, L14302. doi:10.1029/2006GL026140.

Kent, G.M., Babcock, J.M., Driscoll, N.W., Harding, A.J., Dingler, J.A., Seitz, G.G., Gardner, J.V., Mayer, L.A., Goldman, C.R., Heyvaert, A.C., Richards, R.C., Karlin, R., Morgan, C.W., Gayes, P.T., Owen, L.A., 2005. 60 k.y. record of extension across the western boundary of the Basin and Range province: estimate of slip rates from offset shoreline terraces and a catastrophic slide beneath Lake Tahoe. Geology 33, 365–368.

King, G.C.P., Klinger, Y., Bowman, D., Tapponier, P., 2005. Slip-partitioned surface breaks for the Mw 7.8 2001 Kokoxili earthquake, China. Bull. Seismol. Soc. Am. 95, 731–738.

Koehler, R.D., Wesnousky, S.G., 2011. Late Pleistocene regional extension rate derived from earthquake geology of late Quaternary faults across the Great Basin, Nevada, between 38.5° and 40°N latitude. Bull. Geol. Soc. Am. 123, 631–650.

McCaffrey, R., 2002. Crustal block rotations and plate coupling. In: Stein, S.A., Freymueller, J. (Eds.), Plate Boundary Zones. : AGU Geodynamic Series. AGU, Washington, D. C, pp. 101–122.

McQuarrie, N., Wernicke, B.P., 2005. An animated tectonic reconstruction of southwestern North America since 36 Ma. Geosphere 1, 147–172.

Nicholson, C., Seeber, L., Williams, P., Sykes, L.R., 1986. Seismic evidence for conjugate slip and block rotation within the San Andreas fault system, southern California. Tectonics 5, 629–648.

Niemi, N.A., Wernicke, B.P., Brady, R.J., Saleeby, J.B., Dunne, G.C., 2001. Distribution and provenance of the middle Miocene Eagle Mountain Formation, and implications for regional kinematic analysis of the Basin and Range province. Geol. Soc. Am. Bull. 113, 419–442.

Oldow, J.S., Aiken, C.L.V., Hare, J.L., Ferguson, H.G., Hardyman, R.F., 2001. Active displacement transfer and differential block motion within the Central Walker Lane, western Great Basin. Geology 29, 19–22.

Petronis, M.S., Geissman, J., Oldow, J.S., McIntosh, W.C., 2009. Late Miocene to Pliocene vertical-axis rotation attending development of the Silver Peak–Lone Mountain displacement transfer zone, west-central Nevada. In: Oldow, J.S., Cashman, P.H. (Eds.), Late Cenozoic Structure and Evoluton of the Great Basin–Sierra Nevada Transition. Geological Society of America, Denver, pp. 215–253.

Ramelli, A.R., Bell, J.W., dePolo, C.M., Yount, J.C., 1999. Large-magnitude, late Holocene earthquakes on the Genoa Fault, west-central Nevada and eastern California. Bull. Seismol. Soc. Am. 89, 1458–1472.

Rogers, D.K., 1975. The Carson Lineament — its influence on recent left-lateral faulting near Carson City, Nevada. Geological Society of America Abstracts with Programs, 7, p. 1250.

Rood, D.H., Burbank, D.W., Finkel, R.C., 2011a. Spatiotemporal patterns of fault slip rates across the Central Sierra Nevada frontal fault zone. Earth Planet. Sci. Lett. 301, 457–468.

Rood, D.H., Burbank, D.W., Herman, S.W., Bogue, S., 2011b. Rates and timing of vertical-axis block rotations across the central Sierra Nevada-Walker Lane transition in the Bodie Hills, California/Nevada. Tectonics 30.

Sarmiento, A.C., 2010. Earthquake Recurrence and Modes of Deformation in the Central and Northern Walker Lane: Observations from Paleoseismic Trenches Across the Carson and Sierra Nevada Range Fronts. University of Nevada, Reno.

Sarmiento, A.C., Wesnousky, S.G., Bormann, J.M., 2011. Paleoseismic trenches across the Carson and Sierra Nevada rangefronts in Antelope Valley, California and Reno, Nevada. Bull. Seismol. Soc. Am. 101, 2542–2549. doi:10.1785/0120100176.

Saucedo, G.J., Wagner, S.L., 1992. Geologic Map of the Chico Quadrangle California Division of Mines and Geology: Regional Geologic Map Series 7a.

Snow, J.K., Wernicke, B., 1989. Uniqueness of geological correlations — an example from the Death-Valley Extended Terrain. Geol. Soc. Am. Bull. 101, 1351–1362.

Snow, J.K., Wernicke, B.P., 2000. Cenozoic tectonism in the central basin and range: magnitude, rate, and distribution of upper crustal strain. Am. J. Sci. 300, 659–719.

Stewart, J.H., 1988. Tectonics of the Walker Lane Belt, western Great Basin Mesozoic and Cenozoic deformation in a zone of shear. In: Ernst, W.G. (Ed.), Metamorphism and Crustal Evolution of the Western U.S., Ruby Volume VII. Prentice Hall, Englewood Cliffs, New Jersey, pp. 685–713.

Surpless, B.E., 2010. New Constraints on Quaternary slip rates of the Wassuk Range fault system, western Nevada. 106th Geological Society of America Annual Meeting, and Pacific Section, American Association of Petroleum Geologists (27–29 May 2010), Paper No. 12-6.

Taylor, T.R., Dewey, J.F., 2009. Transtensional analyses of fault patterns and strain provinces of the Eastern California shear zone-Walker Lane on the eastern margin of the Sierra Nevada microplate, California and Nevada. Int. Geol. Rev. 51, 843–872.

Thatcher, W., Foulger, G.R., Julian, B.R., Svarc, J.L., Quilty, E., Bawden, G.W., 1999. Present-day deformation across the Basin and Range province, western United States. Science 283, 1714–1717.

Unruh, J., Humphrey, J., Barron, A., 2003. Transtensional model for the Sierra Nevada frontal fault system, eastern California. Geology 31, 327–330.

Wernicke, B., Axen, G.J., Snow, J.K., 1988. Basin and range extensional tectonics at the latitude of Las-Vegas, Nevada. Geol. Soc. Am. Bull. 100, 1738–1757.

Wernicke, B., Davis, J.L., Bennett, R.A., Normandeau, J.E., Friedrich, A.M., Niemi, N.A., 2004. Tectonic implications of a dense continuous GPS velocity field at Yucca Mountain, Nevada. J. Geophys. Res. Solid Earth 109.

Wesnousky, S.G., 2005a. Active faulting in the Walker Lane. Tectonics 24. doi:10.1029/2004TC001645.

Wesnousky, S.G., 2005b. The San Andreas and Walker Lane fault systems, western North America: transpression, transtension, cumulative slip and the structural evolution of a major transform plate boundary. J. Struct. Geol. 27, 1505–1512.

Wesnousky, S.G., Caffee, M.W., 2011. Range-bounding normal fault of Smith Valley, Nevada: limits on age of last surface rupture earthquake and late Pleistocene rate of displacement. Bull. Seismol. Soc. Am. 101, 1431–1437.

Wesnousky, S.G., Jones, C.H., 1994. Oblique slip, slip partitioning, spatial and temporal changes in the regional stress field, and the relative strength of active faults in the Basin and Range, western United States. Geology 22, 1031–1034.